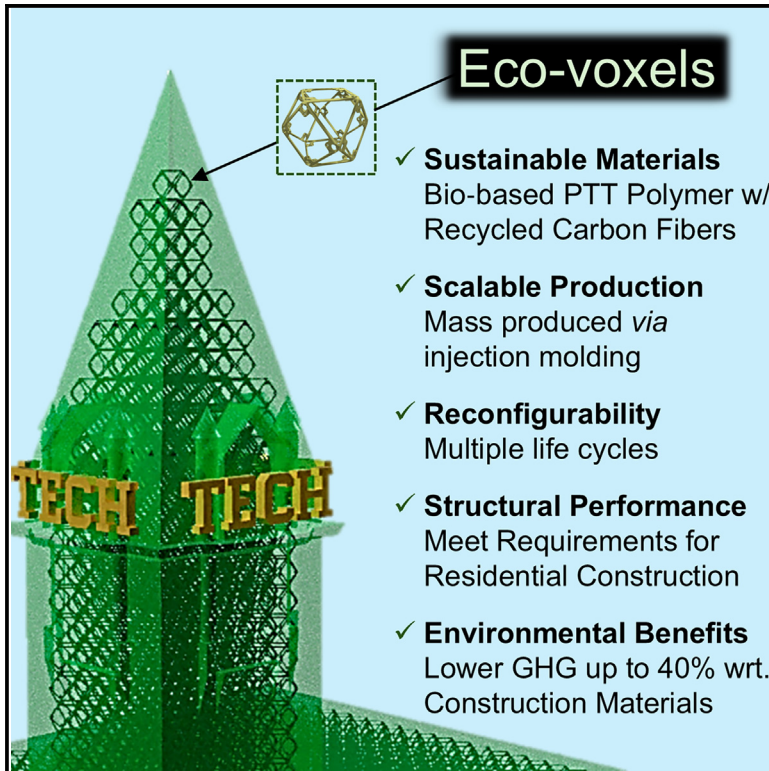


# Eco-voxels: Building blocks for sustainable, load-bearing structures

## Graphical abstract



## Highlights

- Bio-based PTT and rCF sustainable composite material
- Scalable, reconfigurable, and modular structure assembly with automation potential
- Reduction of greenhouse gas emissions by up to 40% compared with traditional methods

## Authors

Dimitrios Georgiou, Daniel Okegbu, Zeshi Yang, ..., Neil Gershenfeld, Wentao Yan, Christos E. Athanasiou

## Correspondence

athanasiou@gatech.edu

## In brief

Eco-voxels contribute to the advent of sustainable construction by introducing load-bearing building blocks that are modular, reconfigurable, and scalable. These components bridge material innovation with environmental responsibility, addressing the challenges posed by contemporary unsustainable conventional methods. Engineered from a partially bio-degradable and recycled composite material and produced at scale, eco-voxels effectively reduce the carbon footprint while meeting required structural performance criteria—as demonstrated in a residential wall case study. This approach motivates the global shift toward sustainable construction.



## Demonstrate

Proof-of-concept of performance with intended application/response

Georgiou et al., 2025, Matter 8, 102106  
July 2, 2025 © 2025 Elsevier Inc. All rights are reserved, including those for text and data mining, AI training, and similar technologies.  
<https://doi.org/10.1016/j.matt.2025.102106>

Article

# Eco-voxels: Building blocks for sustainable, load-bearing structures

Dimitrios Georgiou,<sup>1</sup> Daniel Okegbu,<sup>1</sup> Zeshi Yang,<sup>2</sup> Tao Wang,<sup>3,4</sup> Michael R. Snowden,<sup>3,4</sup> Amar Mohanty,<sup>3,4</sup> Neil Gershenfeld,<sup>5</sup> Wentao Yan,<sup>2</sup> and Christos E. Athanasiou<sup>1,6,\*</sup>

<sup>1</sup>Daniel Guggenheim School of Aerospace Engineering, Georgia Institute of Technology, Atlanta, GA 30332, USA

<sup>2</sup>Department of Mechanical Engineering, National University of Singapore, Singapore 117575, Singapore

<sup>3</sup>Bioproducts Discovery and Development Centre, Department of Plant Agriculture, University of Guelph, Crop Science Building, Guelph, ON N1G 2W1, Canada

<sup>4</sup>School of Engineering, University of Guelph, Thornbrough Building, Guelph, ON N1G 2W1, Canada

<sup>5</sup>Center for Bits and Atoms, Massachusetts Institute of Technology, Cambridge, MA 02139, USA

<sup>6</sup>Lead contact

\*Correspondence: [athanasiou@gatech.edu](mailto:athanasiou@gatech.edu)  
<https://doi.org/10.1016/j.matt.2025.102106>

**PROGRESS AND POTENTIAL** Over centuries, the development of structural materials for construction has primarily focused on improving mechanical performance, but at a significant environmental cost—approximately 10% of global greenhouse gas emissions is attributed to the construction industry, with materials like cement, steel, and concrete accounting for roughly 70% of them. Today, the urgent need for sustainable materials that meet structural performance criteria while minimizing environmental impact is clear. This work introduces eco-voxels: modular, reconfigurable building blocks made from bio-based poly(trimethylene terephthalate) and recycled carbon fibers and produced at scale via injection molding. This research demonstrates that, when applied to standardized residential structures, eco-voxels deliver modularity, reconfigurability, and mechanical performance, while offering a solution to the sustainability challenge by featuring a 15%–40% reduction in carbon footprint compared with conventional methods.

## SUMMARY

The housing and climate crises are intertwined: climate change increases housing costs through increased damage and insurance premiums, while resource-intensive construction boosts greenhouse gas emissions. Emerging alternative construction methods aim to reduce the environmental impact but often rely on materials with questionable sustainability benefits. In this study, we build on the concept of digital metamaterials—lightweight, reconfigurable building blocks—by introducing eco-voxels: modular, mass-producible construction units made from an in-house-developed polymer composite of partially sustainably sourced polymer and rCFs. By assessing the structural performance of an eco-voxel wall, we illustrate the suitability of this construction method for residential buildings. In parallel, by comparing the carbon footprint of a 1 m<sup>2</sup> eco-voxel wall with traditional concrete, three-dimensional-printed concrete, and CLT, we demonstrate 20%–40% reduced greenhouse gas emissions. Our analysis demonstrates that eco-voxels meet load-bearing requirements and offer a reduced carbon footprint aligned with eco-conscious construction demands.

## INTRODUCTION

The global housing crisis and the climate crisis are interconnected. Climate change is affecting housing affordability, as hurricanes, wildfires, and floods of ever-increasing frequency are significantly damaging houses and increasing insurance rates.<sup>1</sup> Almost 30% of the global urban population lives in slums,<sup>2</sup> while by 2025, 440 million urban households worldwide are expected to occupy crowded, inadequate, and unsafe housing or be finan-

cially stretched by housing costs.<sup>3</sup> This is not only due to climate change. Rising land prices and regulatory constraints on development lead to housing shortages and higher prices and rents.<sup>4</sup> In parallel, the growing need for resources to house the expanding global population puts a heavy burden on the climate. Building construction accounts for 6% of global energy consumption and 10% of global greenhouse gas (GHG) emissions.<sup>5</sup> Production of concrete, the most extensively used building material, has increased 30 times in the last 75 years, accounting for 8%

of global CO<sub>2</sub> emissions.<sup>6–8</sup> In addition, a significant amount of waste is generated from buildings construction and demolition, with 600 million tons of such debris being generated in the United States annually—more than twice the amount of municipal solid waste.<sup>9</sup>

In recent years, a number of alternative construction methods have emerged to address these challenges, including three-dimensional (3D) concrete printing and modular building panels made from lightweight polymer composites or cross-laminated timber (CLT), an engineered wood product made by layering timber sheets in alternating directions and bonding them under pressure. These construction approaches can significantly lower construction times and reduce labor needs, hence providing cheaper housing options. They can also generate less waste and create fewer disturbances on construction sites compared with traditional building approaches.<sup>10</sup> Furthermore, modular buildings can be disassembled and relocated or refurbished, reducing the need for virgin materials and energy.<sup>11</sup>

Given the significant benefits of modular construction methods, extensive research has focused on this area. Among these emerging approaches, digital metamaterials<sup>12–14</sup> stand out as a promising innovation for enabling the construction of large, load-bearing, reconfigurable structures assembled from discrete building blocks. The term digital metamaterials describes a system of discrete components, called voxels, each corresponding with specific relative positions and orientations.<sup>13</sup> Voxels form modular and reconfigurable structures featuring lattice designs, which offer scalability advantages through advanced manufacturing methods, rapid component production, and the capability for automated assembly.<sup>14–17</sup>

However, the environmental trade-offs of alternative construction methods over conventional ones remain questionable, as the building materials used are very limited and unsustainable, dominated by concrete, cement-based materials, or fossil-based thermoplastic composites. For example, printable concrete mixtures require more cement and fly ash to ensure the stability of printed structures, increasing significantly the generation of CO<sub>2</sub> emissions,<sup>18</sup> and, although digital metamaterials can optimize stiffness-to-weight ratios, existing approaches rely on glass-fiber-reinforced virgin polymers.<sup>14</sup> Wood is the only renewable material widely employed in modular construction methods, but the environmental benefits of mass timber are debated due to concerns about forest management practices, and CO<sub>2</sub> emissions from logging, manufacturing, and transportation of wood products.<sup>19</sup>

Existing sustainable materials, such as bio-based polymer composites and bamboo, often fail to provide the necessary structural performance or are hindered by limited availability and inconsistent supply chains,<sup>20–22</sup> making them unsuitable for large-scale, load-bearing structures.<sup>23–25</sup> In this paper, we address these challenges by proposing a solution that combines modularity with sustainability: load-bearing structures made from eco-friendly materials. Using the digital metamaterial approach, we developed discrete building blocks called eco-voxels, made from a blend of polytrimethylene terephthalate (PTT) polymer and recycled carbon fibers (rCFs). As a case study, we evaluated the structural performance of a 1 m<sup>2</sup> eco-voxel external load-bearing wall for a one-story residential

building in the United States, designed according to the American Society of Civil Engineers (ASCE) standards.<sup>26</sup> Harnessing advances in finite element methods (FEMs) and computational power, we optimized and assessed the eco-voxel wall structure through calibrated computational models, significantly reducing the need for extensive physical testing. Additionally, we compared its carbon footprint and mass with those of a concrete masonry wall, a 3D-printed concrete wall, and a CLT wall of similar load-bearing capacities (cradle-to-gate, structural perspective). An overview of the performed work is shown in [Figures 1A–1D](#). Overall, this study demonstrates an eco-friendly construction method that merges the advantages of modular construction with recent advances in computational modeling and sustainable material development.<sup>27</sup> This approach could potentially enable future reconfigurable structures of multiple life cycles ([Figures 1E and 1F](#)).

## RESULTS

### Sustainably sourced composite material: PTT + rCFs

Our goal was to identify a polymer composite material that could match the mechanical properties of virgin nylon glass fiber reinforced composite (GFRP) used in [Jennett et al.<sup>14</sup> \(Table 1, row 6\)](#), while incorporating a significant fraction of renewable and/or recycled feedstocks to minimize environmental impact. We aimed for a sustainably sourced material that would not compromise the structural integrity required for the intended application. However, after an extensive search for commercially and readily available materials containing at least 10 wt % sustainably sourced content, we found that none of the available options met or exceeded the mechanical performance of GFRP (see examples in [Table 1](#)).

To that end, we developed a composite material blending 80 wt % PTT thermoplastic polymer, which is 35% sourced from corn sugar,<sup>35</sup> and reinforced with 20 wt % rCF recovered mostly from aerospace scrap through pyrolysis.<sup>36</sup> The rCFs were coated with polyurethane to facilitate compounding and improve adhesion.<sup>37,38</sup>

PTT offers a wide range of desirable properties that make it suitable as an engineering thermoplastic.<sup>39,40</sup> Its advantages include excellent physical strength, chemical resistance, low moisture absorption, dimensional stability, ease of processing, and recyclability.<sup>39–42</sup> In parallel, rCFs offer significant sustainability benefits by reducing waste and lowering the carbon footprint compared with virgin carbon fibers, as their production requires less energy and fewer raw materials.<sup>43</sup> Structurally, they retain a considerable portion of the mechanical properties of virgin fibers, making them a viable option for reinforcing composites in load-bearing applications, while contributing to circular economy practices. The properties of the developed PTT and rCF composite are presented in [Table 2](#).

### Eco-voxels design and manufacturing

For the eco-voxels, we used the design that was introduced by [Jennett et al.<sup>14</sup>](#) Each eco-voxel is a cuboctahedron composed of six square-shaped face parts. The face parts are assembled using rivets to form a complete cuboctahedral eco-voxel. Once assembled, multiple eco-voxels are connected through

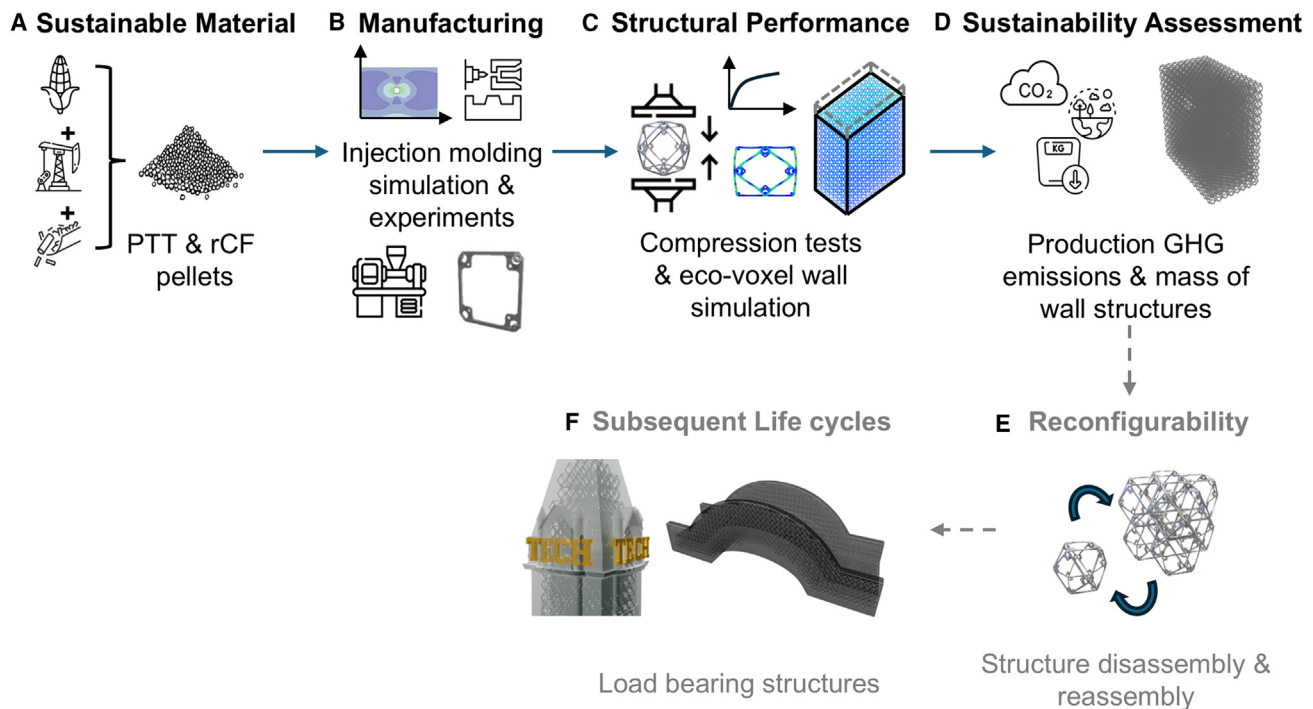


**Figure 1. Overview of the work performed and future potential of the digital eco-voxel-based construction method**

(A) Development of a 48 wt % sustainably sourced polymer composite, derived from PTT, partially sourced from bio-based feedstock and reinforced with rCFs. (B) Manufacturing of eco-voxels via injection molding, with processing parameters optimized through simulations for the developed composite material. (C) Compression testing of individual eco-voxels, providing data to inform simulations and models of the load-bearing capacity of multi-voxel structures. (D) Assessment of GHG emissions and mass associated with the production of a 1 m<sup>2</sup> eco-voxel, external load-bearing wall of a one-story residential building in the US, compared with walls of similar functionalities made from conventional and alternative construction methods. (E) The eco-voxel wall structure is reconfigurable,<sup>17</sup> allowing it to be disassembled and reassembled to create subsequent load-bearing structures (Video S1). (F) Potential for multiple life cycles of eco-voxels enabled by their reconfigurability. Dotted arrows and gray text in (E) and (F) indicate future potential that has not yet been explored or demonstrated in the current work.

inter-voxel joints, allowing the formation of larger structures (Note S1 and Figure S1).

Injection molding was used for manufacturing the eco-voxel faces (Note S2 and Figures S2–S4), as it offers lower per-unit costs and faster production speeds for the mass production of modular structure parts compared with other approaches, e.g., 3D printing.<sup>14</sup> It ensures high repeatability and consistency, producing precise, uniform parts with minimal variation, which is essential for modular structures that need to fit together precisely.<sup>44</sup>

However, injection molding of new materials requires optimization of processing parameters to ensure high-quality parts and performance.<sup>45,46</sup> Factors like temperature, pressure, and cooling time must be carefully adjusted to suit the material’s specific characteristics, such as its flow behavior, melting point, and shrinkage rate. Improper settings can lead to defects like warping, incomplete fills, or heterogeneity in final parts. By fine-tuning these parameters, optimized material flow can be achieved, minimizing defects and ensuring our material’s potential is fully realized in the final products. The mechanical properties of PTT are particularly sensitive to processing conditions, such as mold temperatures,<sup>40,47</sup> and this sensitivity increases when working with PTT composites as is the case in this work. Therefore, precise control of processing parameters is critical.

To achieve this, we combined trial-and-error experimentation with high-fidelity direct numerical simulations of the injection molding process for the eco-voxel’s faces. We conducted injection molding using various combinations of processing and mold temperatures, holding and injection pressures, cooling times, and shot sizes, and then characterized the resulting specimens using sub-micron computed tomography (Figure S3). Simultaneously, we analyzed the behavior of viscoelastic polymer flows using a high-fidelity computational fluid dynamics model solving fluid dynamics and heat transfer equations (see [eco-voxel manufacturing experiments and simulation](#)).

We compared two flow behaviors under different assumptions: constant viscosity and strain rate-dependent viscosity. The strain rate-dependent viscosity, modeled using a non-Newtonian approach, exhibited more nuanced behavior in areas of complex flow, particularly around corners and thin sections of the eco-voxel face. Viscosity was influenced by both strain rate and temperature, leading to more complex flow patterns, as shown by the varying viscosity distributions (Figures S4A and S4B). This integrated approach allowed us to reduce physical trial-and-error iterations, while identifying the optimal processing conditions and material flow rates to achieve homogeneous parts (Table 3; Figure S4C).

**Table 1. Properties of commercially available and sustainably sourced materials (rows 1–5) compared with those of reference material (row 6)**

No	Candidate Material	Tensile Strength [MPa]	Young's Modulus [GPa]	Vendor
1	nylon with maple composite (Terratek WC200180)	72.5	4	Greendot Bioplastics <sup>28</sup>
2	recycled PEEK resin (Ketron Sterra 1000 PEEK)	115	4.3	Ketron, Mitsubishi Chemical Group <sup>29</sup>
3	recycled PEEK glass fiber composite (PK 150G30)	199.9	8.5	The Resin Enterprise <sup>30</sup>
4	PLA resin (Ingeo Biopolymer 3052D)	62	3.6	NatureWorks <sup>31</sup>
5	P3HB resin	40	3.5	Mango Materials <sup>32,33</sup>
6	reference material: GFRP (Zytel 70G33L BK031)	140–200	10.5	DuPont <sup>34</sup>

P3HB, poly-3-hydroxybutyrate; PEEK, polyether ether ketone; PLA, polylactic acid.

### Structural performance of eco-voxel load-bearing wall

We sought to design and evaluate the structural performance of a 1 m<sup>2</sup> load-bearing eco-voxel wall for a one-story residential building in the United States, enabling a direct comparison with other construction methods. The wall's thickness was determined through structural analysis simulations, based on the specific loads it must withstand. To ensure the accuracy of the structural model, we first needed to validate it by simulating the performance of smaller lattice structures under compression, using both experimental testing and highly accurate modeling techniques.

Assessing the structural performance of lattice structures through simulations has become increasingly precise and efficient. Advances in FEM, optimization techniques, and computational power enable the accurate simulation of large-scale structures by calibrating computational models with data from experimental tests on small-scale configurations. This approach significantly reduces the need for extensive physical testing, which is now primarily used for calibrating and validating these computational models.<sup>48–57</sup> Therefore, the structural performance of eco-voxel lattices with side lengths where the voxel count was  $n \leq 3$  was experimentally characterized through compression tests which were then used to calibrate the FEM simulations (Figure 2).

FEM simulations can be performed using full 3D models. However, these models become computationally prohibitive for structures with more than a million elements, which is the case for eco-voxel lattices with side lengths where the voxel count exceeds 2, as in the eco-voxel wall. In such cases, reduced-order beam element models (ROMs) can be employed. Eco-voxels with intermediate connectivity ( $Z = 8$ ) exhibit stretch-dominated behavior<sup>14,56</sup> (Note S3 and Figure S5) and feature rigid nodes that enhance their effective stiffness. As a result, global stiffness and strength are primarily governed by the beam struts, allowing the eco-voxel lattices to behave as networks of interconnected beams. Therefore, the ROM approach could be employed to accurately capture the structural behavior of the eco-voxel wall, while significantly reducing computational costs. To validate the ROM model's accuracy, we simulated the stress-strain curves and deformation patterns of  $2 \times 2 \times 2$  and  $3 \times 3 \times 3$  eco-voxel lattices using both ROM and full 3D modeling and calibrated the models with the experimental data obtained (Figure 2). The effective stress-strain curves from both the full 3D model and the ROM exhibit the typical behavior of a cuboctahedral voxel: an initial linear region, followed by softening as both the vertical and inclined struts bend or buckle, and localized yielding at the connecting nodes signaling the stress limit of the structure.<sup>14,58</sup> For all cases, the effective stress is defined as the applied load divided by the projected square cross-sectional area. Effective strain is defined as the vertical displacement divided by the original height

**Table 2. Properties of the sustainably sourced composite material**

Property	Value
Density [g/cm <sup>3</sup> ]	1.35
Ultimate tensile stress [MPa]	163 ± 6.2
Yield stress [MPa]	104 ± 4.1
Young's modulus [GPa]	20.6 ± 1.1
Elongation at break [%]	1.7 ± 0.2
Flexural modulus [GPa]	14.5 ± 0.6
Flexural strength [MPa]	240 ± 5.7
Notched Izod impact strength [J/m]	80 ± 11
Heat deflection temperature [°C]	220
Melt flow index [g/10 min]	9 ± 0.2

**Table 3. Optimal processing parameters for the injection molding of eco-voxel parts**

Parameter	Value
Processing/barrel temperature [°C]	260
Mold temperature [°C]	30–35
Holding pressure [MPa]	6.2
Injection pressure [MPa]	8.3
Cooling time [s]	60
Shot size [mm]	60
Flow rate [g/s]	17.4

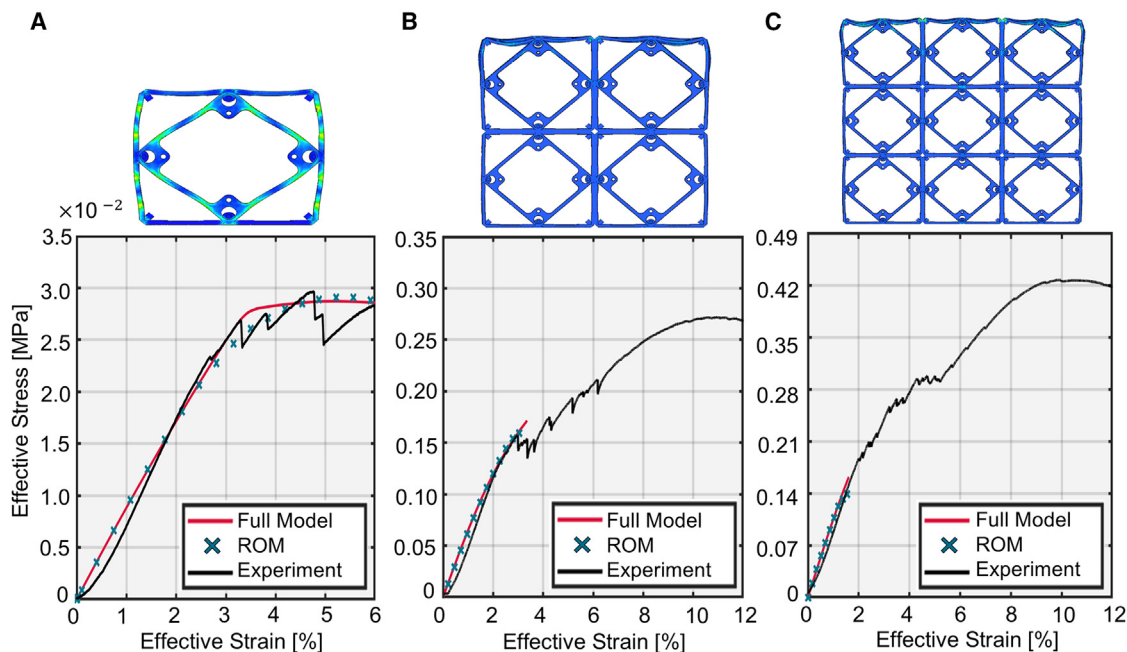


**Figure 2. Development of the eco-voxel wall structural analysis model through experiments, full 3D modeling, and ROM**

(A) Effective stress-strain curves and deformation patterns of a single eco-voxel under compression.

(B) Effective stress-strain curves and deformation patterns of a  $2 \times 2 \times 2$  eco-voxel lattice under compression.

(C) Effective stress-strain curves and deformation patterns of a  $3 \times 3 \times 3$  eco-voxel lattice under compression. The FEM simulations include the effect of geometric nonlinearity due to large deformations. The stress drops observed during the experiment indicate progressive failure of the struts caused by buckling followed by strain softening, as the structure gradually loses stiffness.

of the structure from the bottom to the top face nodes. The results show strong agreement between the computational and experimental data, with both models accurately capturing the point of strut failure, here defined as the point at which at least one strut either buckles or yields. Evident non-linearity in the near the yield/buckle point exhibited in the FEM response, especially in the  $1 \times 1 \times 1$  case, is attributed to the effect of geometric nonlinearity and large deformations (see [methods](#)). Even in the single-voxel case (Figure 2A), where the model is prone to large deformations and instabilities, the linear regime of the response remains well aligned with experimental results. The stress drops observed indicate progressive failure of the beam struts due to buckling. Moreover, this drop is followed by strain softening, as the structure gradually loses stiffness. Since the stiffness of a voxel structure can be modeled as a connected network of springs,<sup>14</sup> the failure of a single strut reduces the overall load-bearing capacity, leading to progressive stiffness loss. As the number of voxels increases (Figures 2B and 2C), the structure becomes stiffer, exhibiting an increasingly linear response at small strains. Deviations from linearity in the small strain regime are attributed to minor joint slipping caused by metal fasteners within their sockets. Unlike the single-voxel experiment, where progressive strut failure can lead to immediate instability, larger structures retain their load-bearing capacity as intact struts continue to carry the load.<sup>57</sup> This distribution enhances yield and maximum stress, as the load is shared across more struts, while stiffness degradation, though present in all cases, becomes less pronounced with increasing structure size.

While the eco-voxel lattices are primarily designed for load-bearing applications under compression, their behavior under tensile loading is expected to follow a similar pattern. Due to the double symmetry of the voxel faces, the deformation mechanisms resemble those observed in compression, with the struts acting as beam-like elements subjected to bending and axial forces. The response typically consists of an initial linear elastic region, followed by progressive strut failure accompanied by strain softening.<sup>14,59</sup> Such tensile responses have been observed in lattice structures with similar geometric symmetries, indicating that this behavior is consistent with established structural trends.<sup>60,61</sup>

The analysis of small-scale structures streamlined the application of ROM for larger lattice structures, demonstrating positive scaling of mechanical properties with a consistent stretch-dominated deformation pattern.<sup>58</sup> Establishing this consistency was crucial for evaluating the large-scale eco-voxel wall. To assess the structural performance of the eco-voxel wall, we modeled the loads required for a load-bearing wall in a one-story residential building in the United States, according to ASCE7 standards.<sup>26</sup> We accounted for both vertical compressive forces from roof and snow loads ( $V$ ) and lateral forces exerted by wind ( $W$ ). Specifically, the worst-case distributed downward load  $V$  was defined as  $V = 1.60 D + 0.75 S$ , where  $D$  represents the dead load (the weight of the roof supported by the wall) and  $S$  the snow load. The distributed load  $W$  was used to simulate the wind effect (Figure 3A; Table 4). The wall is assumed to carry one-half of the vertical load, with an additional safety factor of

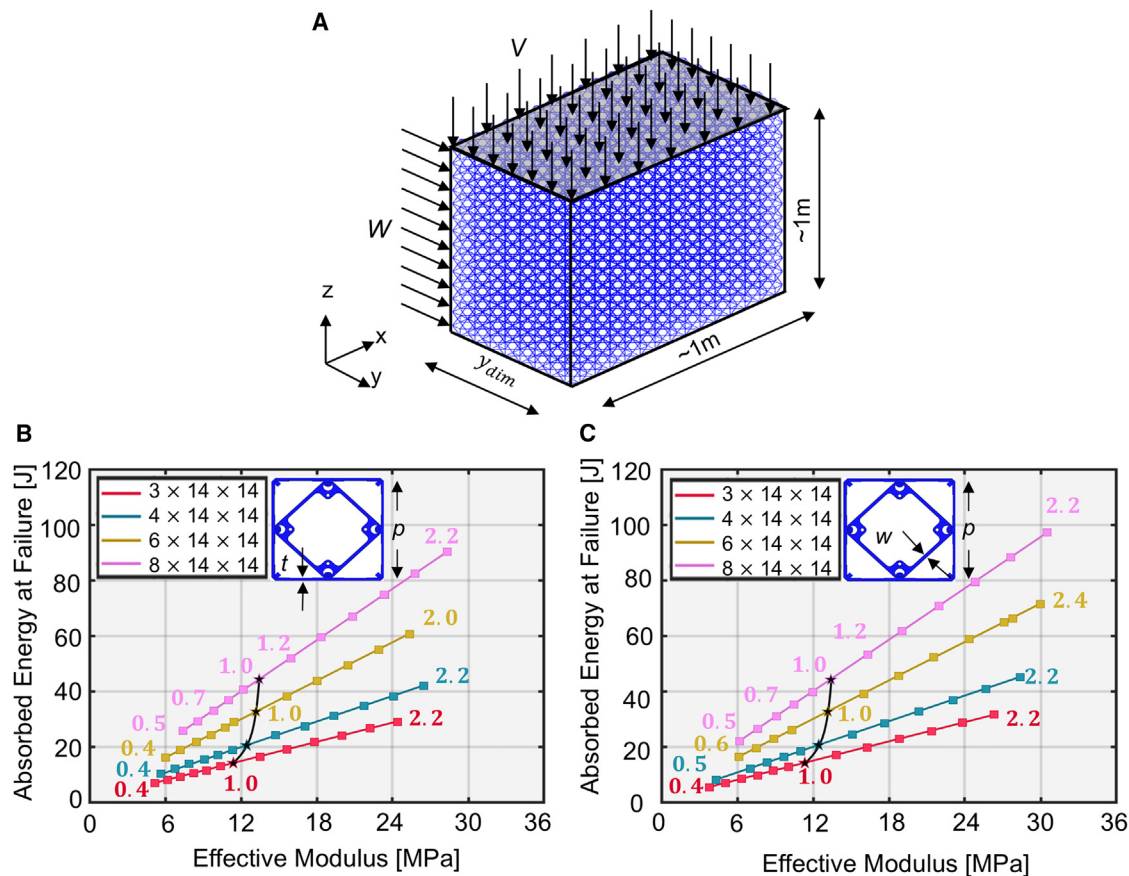


**Figure 3. Structural performance of a 1 m<sup>2</sup> eco-voxel wall**

(A) Schematic of eco-voxel wall with varying widths ( $y_{dim} = 3, 4, 6, 8$ ) subjected to vertical compressive forces from roof and snow loads ( $V$ ), and lateral wind loads ( $W$ ).

(B) Parametric study of eco-voxel wall configurations with varying  $y_{dim}$ , and thickness,  $t$ . We tested a minimum of 12  $t$  combinations for each wall width configuration, ranging from 0.5 to 2 times the baseline values by incrementally increasing  $t$  by 0.1 before the baseline configuration and by 0.2 after the baseline configuration. The baseline configurations are highlighted with black star markers for easy reference.

(C) Parametric study of lattice wall configurations with varying  $y_{dim}$  and voxel width,  $w$ . We tested a minimum of 12  $w$  ranging, for each wall width configuration, from 0.5 to 2 times the baseline values by incrementally increasing  $w$  by 0.1 before the baseline configuration and by 0.2 after the baseline configuration. The baseline configurations are highlighted with black star markers for easy reference. The term baseline refers to walls with the corresponding  $y_{dim}$  that consist of voxels with the same geometry as in Jenett et al.,<sup>14</sup> which was also used to evaluate the structural performance of the wall (Table 5).

2 applied to account for hazardous conditions. We first evaluated the lattice wall's behavior under vertical loading alone and then assessed its performance under combined vertical and lateral loading conditions.

We defined the number of voxels along the  $x$ ,  $y$ , and  $z$  axes as  $x_{dim}$ ,  $y_{dim}$ , and  $z_{dim}$ , respectively. To simulate the performance of 1 m<sup>2</sup> of the eco-voxel wall, the wall's length and height were known and equal to  $x_{dim} = 14$  ( $\approx 1$  m) and  $z_{dim} = 14$  ( $\approx 1$  m), while the optimal width  $y_{dim}$  was under investigation to ensure it could adequately sustain the applied loading conditions,  $V$  and  $W$ . We tested four cases with width values ranging from 5 ( $\approx 0.4$  m) to 8 ( $\approx 0.6$  m). A displacement-controlled loading condition was applied to the top of the wall. Once the stress state of the wall was established, traction at the load-application boundaries was calculated.<sup>51</sup> The yield load for each eco-voxel wall configuration was defined as the point at which the von Mises stress

within any eco-voxel beam exceeded the material's yield stress (Table 2). For an eco-voxel wall configuration to meet the desired structural performance, its yield load must exceed the applied loads; specifically, the ratio of yield load to applied load should be  $>1$ . This condition is satisfied for eco-voxel wall configurations with widths of six eco-voxels or greater (Table 5). We also observed that beyond  $y_{dim} = 6$ , the increase in yield stress becomes marginal (increase  $<10\%$ ).

We conducted a sensitivity analysis on the eco-voxel's beam width ( $w$ ) and thickness ( $t$ ) to assess their influence on wall stiffness and energy absorption (Figures 3B and 3C). The insights from this analysis can guide future designs with narrower wall widths, optimizing material use while enhancing structural integrity. We tested a minimum of 12  $w$  and  $t$  combinations for each wall width configuration (Figures 3B and 3C), ranging from 0.4 to 2.2 times the baseline values, with the baseline marked by

**Table 4. Parameters used for the eco-wall's structural analysis**

Parameter	Value
Dead load, $D$ [N/m <sup>2</sup> ]	670
Snow load, $S$ [N/m <sup>2</sup> ]	2,400
Total vertical load, $V$ [N/m <sup>2</sup> ]	2,870
Lateral load, $W$ [N/m <sup>2</sup> ]	680
Wall thickness, $y_{dim}$ [No. of eco-voxels]	5–8
Wall height, $z_{dim}$ [No. of eco-voxels]	14
Wall length, $x_{dim}$ [No. of eco-voxels]	14
Eco-voxel pitch, $p$ [mm]	77.4
Eco-voxel's beam width, $w$ [mm]	2.38
Eco-voxel's beam thickness, $t$ [mm]	2.26

black star points. Narrower wall width ( $y_{dim} = 3, 4, 6, 8$ ) values than those in the baseline were considered. The values of  $t$  and  $w$  are incrementally increased by 0.1 before the baseline configuration and by 0.2 after the baseline configuration. The term baseline refers to walls with the corresponding  $y_{dim}$  that consist of voxels with the same geometry and dimensions as in Jenett et al.,<sup>14</sup> which was also used to evaluate the structural performance of the wall (Table 5). Holding the beam  $w$  and  $t$  constant, we observed that energy absorption at yield increased proportionally with eco-voxel wall thickness. Absorbed energy at yield is defined as the amount of energy absorbed by the wall before it reaches the yield point during compression. Results show a linear relationship between wall effective stiffness and energy absorption, with the effective stiffness increasing as the beam becomes less slender. Adjustments to the beam's  $t$  or  $w$  shifted the results accordingly, highlighting the strong influence of these dimensions on the eco-voxel wall effective stiffness and energy absorption. These findings could inform the optimization of the eco-voxel wall's effective stiffness-to-mass ratio for more efficient designs.<sup>62</sup>

### Sustainability assessment of eco-voxel load-bearing wall

We assessed the sustainability of the eco-voxel wall using as key metrics the GHG emissions generated during materials production and wall manufacturing, as well as the structure's mass. One square meter of eco-voxel wall was compared with a concrete masonry wall, a 3D-printed concrete wall, and a CLT wall of similar load-bearing capacities from a cradle-to-gate, structural perspective (Figure 4). The concrete wall is made of hollow concrete masonry blocks, reinforced by two concrete columns and one beam with steel rebar and has a 30-cm thickness. The 3D concrete wall uses a high-performance concrete consisting of ordinary Portland cement, fly ash, river sand, polypropylene microfibrils, alkali-free accelerators, and super-plasticizers. The CLT wall consists of wood panels made by bonding layers of

**Table 5. Stress at failure and safety factor of walls with different width,  $y_{dim}$**

Wall width ( $y_{dim}$ )	5	6	7	8
Stress at yield [MPa]	16.21	29.60	32.14	34.25
Yield to applied load ratio [–]	0.97	1.09	1.38	1.53

solid-sawn timber. Each layer is oriented perpendicular to the one below it and glued along the wide faces, typically in a symmetric configuration to ensure that the outer layers align with the same grain direction.

As shown in Figure 4, the concrete masonry wall has the highest GHG emissions, at approximately 130 kg CO<sub>2</sub>-equivalents (CO<sub>2</sub>-eq), followed by the 3D-printed concrete wall at around 125 kg CO<sub>2</sub>-eq, and the CLT wall at roughly 100 kg CO<sub>2</sub>-eq. The eco-voxel-based wall exhibits the lowest GHG emissions, estimated at 80 kg CO<sub>2</sub>-eq—over 30% lower than the concrete walls and about 20% lower than the CLT wall. Additionally, there is a significant variation in the mass of the walls: the concrete wall is the heaviest at approximately 400 kg, while the eco-voxel wall is the lightest at around 16 kg.

These results demonstrate that adopting the eco-voxel approach can lead to substantial reductions in GHG emissions while maintaining the required structural integrity for residential construction. Furthermore, the lightweight nature of the eco-voxel wall can contribute to additional environmental savings during manufacturing and reduce overall construction costs.

We acknowledge that the current eco-voxel wall structure does not include the same environmental barriers or insulation functions as concrete and CLT walls. Our comparison focuses solely on structural components, ensuring equal mechanical performance across structures. A more comprehensive comparison of the functional performance of the three wall systems would require the inclusion of a skin for the eco-voxels material. Although this is beyond the scope of the present study, the 20%–40% lower GHG emissions of eco-voxels walls compared with concrete and CLT ones provide sufficient margin to assume that even with the incorporation of a sustainably sourced or recycled skin, the eco-voxel approach would perform better from an environmental sustainability perspective.

## DISCUSSION

### Safety considerations, stability, and long-term behavior of eco-voxel structures

The structural performance of the eco-voxel wall depends on both the structural design and the material properties. Three key aspects should be considered: safety factors and their scaling with respect to the structure size, structural stability and post-yield behavior, and the long-term creep behavior of the thermoplastic composite eco-voxels.

In this study, we presented a case with a 1 m × 1 m wall to streamline the scalability of our results. In practice, residential walls typically reach 2.5 m in height (~35 voxels), with lengths ranging from 2 m (~28 voxels) to 20 m (~280 voxels). Increasing these dimensions inherently enhances the structure's stiffness and resistance to buckling, as the critical buckling load scales with stiffness. Moreover, as demonstrated in Figure 3, further improvements in the load capacity of the wall can be achieved by optimizing voxel parameters face and adjusting the wall width ( $y_{dim}$ )—potentially reducing it while slightly increasing mass. Additionally, the applied loads in this study were conservatively chosen, applying a safety factor of 2 to the vertical downward load to reflect worst-case conditions and ensure the framework's practical applicability in construction.

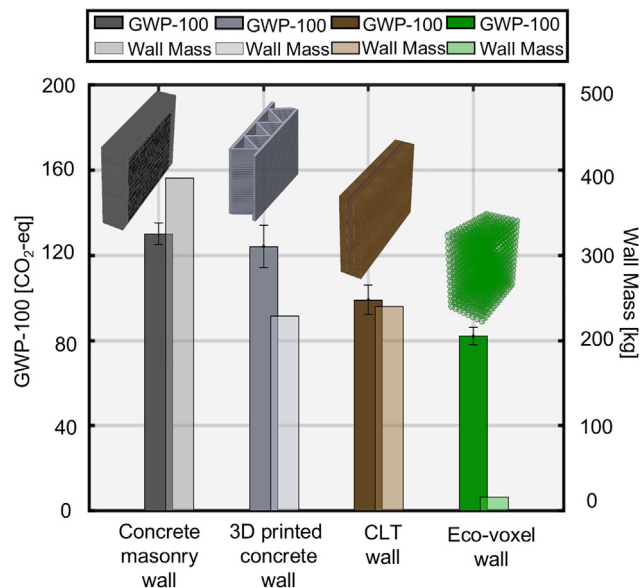


**Figure 4. Sustainability assessment**

GHG emissions (solid color) and wall mass (transparent color) of the eco-voxel wall compared with a concrete masonry wall, a 3D-printed concrete wall, and a CLT wall of similar load-bearing capacities.

The sensitivity of the eco-voxel wall to defects was assessed up to the yield point with less focus on the post-yield behavior. The wall design prioritizes avoiding yielding to minimize the risk of failure, making the post-yield response less critical for the current framework. Experimental tests (Figure 2) demonstrated that the voxel geometry and connectivity primarily lead to buckling and plastic yielding. Even after some isolated failure events, the structure maintains its load-bearing capacity. This aligns with established findings on stretch-dominated lattice structures, where the expected post-yield response typically involves strain softening over a wide strain range until densification occurs, at which point the structure resists further deformation unless subjected to excessive force.<sup>14,51,57,58</sup> Therefore, the mechanical response of the eco-voxels permits their use within our sustainable construction framework.

Long-term performance of such a polymer-based eco-voxel structure will be influenced by complex thermomechanical phenomena, e.g., creep deformation. Thermoplastics like PTT are susceptible to creep but reinforcing the polymer with rCF significantly improves its resistance and are suitable for load-bearing applications such as automotive flooring and structural guards.<sup>63</sup> Although we expect our structure to maintain integrity under prolonged loading periods,<sup>64,65</sup> further mechanical testing would be needed to extract detailed material properties under various environments and loading scenarios.<sup>66–71</sup>

### Integrating eco-voxels into construction

Our PTT-rCF composite is an emerging sustainable material with increasing availability due to growing recycling efforts and industrial demand. Currently, 30% of carbon fiber produced becomes waste (~31,200 metric tons/year), yet only 15% is recycled, leaving room for expansion.<sup>72,73</sup> The global rCF market, valued at

US\$151.1 million in 2023, is projected to reach US\$297 million by 2030 (CAGR 8.8%), with improved recycling technologies driving supply. PTT, widely used in textiles and automotive applications, is also expanding, with a market value of US\$896.8 million in 2021 and a projected US\$1.41 billion by 2030 (CAGR 5.4%).<sup>74</sup> Specifically, in 2024, North America's PTT market was valued at US\$134.8 million, while East Asia held a 22.4% market share, reflecting rising global demand.<sup>75</sup> Therefore, while PTT-rCF composites currently lag behind GFRP, concrete, and wood in availability, advancements in fiber recovery and bio-based polymers are expected to scale production, positioning it as a viable, low-impact alternative to conventional materials.

Although the primary focus of this study is on the structural performance of the eco-voxel wall, its insulation capacity is an important consideration for future research. This could be achieved by incorporating insulation materials or protective skins, e.g., polyurethane foams or mineral wool, which disrupt conductive and convective heat transfer.<sup>76,77</sup> Additionally, bio-based alternatives such as cellulose or hemp fibers could offer promising insulation properties with minimal environmental impact.<sup>78</sup> These materials are lightweight and would not significantly affect the mechanical performance of the wall. The modular design of the eco-voxel structure allows for insulation to be incorporated internally, externally, or within the voxel cavities, depending on performance requirements.

### Conclusion

This study demonstrates a sustainable construction approach through the development of load-bearing walls made from modular building blocks composed of eco-friendly materials. By integrating the principles of digital metamaterials with advanced computational modeling and sustainable material design, eco-voxels offer a lightweight, low-emission alternative to traditional construction approaches, without compromising structural integrity, making them well-suited for rapid and scalable applications (Video S1). Potential uses include space structures and emergency shelters for disaster relief scenarios such as hurricanes, earthquakes, wars, and pandemics, where quick assembly, modularity, and minimal environmental impact are crucial.

Future work could improve this initial eco-voxel design by refining its geometry to meet specific stiffness-to-mass targets and by redesigning the intra-voxel connections to eliminate the need for fasteners. Additionally, a comprehensive cradle-to-grave environmental impact assessment—covering aspects like transportation, usage, and end of life—would offer a more thorough understanding of the environmental footprint of our approach. Finally, further research is necessary to address practical considerations such as insulation, protective cladding, and durability under diverse environmental conditions, ensuring their practicality in real-world applications.

### METHODS

#### Material development

The sustainably sourced composite material is partially bio-based poly(trimethylene terephthalate) (SORONA FG3301 NC010, DuPont, Wilmington, DE, USA), with 35 wt % renewable content

derived from corn, reinforced with 20 wt % rCFs (Barnet-Carbon CF82-PU from William Barnet and Son, LLC, Spartanburg, SC, USA) featuring an average fiber length of 6 mm and filament diameter of 5  $\mu\text{m}$ , coated with polyurethane (sizing content 1.4 wt %). The PTT unfilled polymer resin was kindly donated by DuPont and acquired in pellet form.

PTT is a polyester that is prone to hydrolysis during processing, so it was pre-dried in an oven at 80°C for at least 4 h to reduce moisture content to <0.2%. The composite material was prepared using a LabTech (Model L5E26-32, LabTech Engineering Co. LTD, Samutprakarn, Thailand) co-rotating twin screw extruder at 70–80 rpm at a temperature of 250°C. The strands were cooled in a water bath before being pelletized. To prepare mechanical test samples, the pellets were injection molded with a Mini-Injector model 55P (Electro-Matic, Farmington Hills, MI, USA) at a temperature of 270°C.

Before testing, the samples were conditioned according to American Society for Testing and Materials (ASTM) standard D618.<sup>79</sup> Tensile testing was performed according to ASTM D638 sample type IV at 5 mm/min,<sup>80</sup> and flexural testing at 1.4 mm/min according to ASTM D790 procedure A,<sup>81</sup> using a Universal Testing Machine (Instron model 3382, Norwood, MA, USA). The presented results are the average of five measurements, analyzed using Instron Bluehill software (Note S4 and Figure S6). Notched Izod impact testing was performed using a Zwick/Roell HIT25P Plus (ZwickRoell, Ulm, Germany) according to ASTM D256 method A<sup>82</sup> at 23°C, with each reported value being the average of six samples. Heat deflection temperature was measured using a Q800-DMA instrument (TA Instruments, New Castle, DE, USA) at 0.455 MPa load, following ASTM D648<sup>83</sup> and.<sup>84</sup> A melt flow indexer 2000A (Qualitest USA, Plantation, FL, USA) was used to measure the melt flow rate or index according to ASTM D1238.<sup>85</sup> Density was measured using an MDS-300 densimeter (Qualitest USA).

### Eco-voxel manufacturing experiments and simulation

The eco-voxel face mold was designed in Rhinoceros 3D computer-aided design application software (Robert McNeel & Associates - TLM, Inc., Seattle, WA, USA). A two-part mold (Figure S2) was machined from multipurpose 6061 aluminum plates of 3.8 cm thickness, 12.7 cm width, and 15.2 cm length (McMaster-Carr, Elmhurst, IL, USA) via computer numerical control machining (HAAS VF1, HAAS Automation, Oxnard, CA, USA). The eco-voxel parts were manufactured using a Sumitomo EI-Exis SP 150/500 injector molder (Sumitomo, Tokyo, Japan). The optimal injection process parameters are presented in Table 3. Molded parts underwent sub-micron computed tomography using Rigaku nano3DX (Rigaku, Tokyo, Japan). Eco-voxel parts were assembled with 2.38-mm diameter blind aluminum rivets (McMaster-Carr), using a pneumatic rivet gun, following Jennet et al.<sup>14</sup>

The high-fidelity direct numerical multi-physics model incorporated both constant and strain-rate dependent viscosity, exploring the impact of these variables on the mold-filling process. The computational domain was created from an STL file and meshed with 2.15 million elements at a mesh size of 0.2 mm, ensuring detailed resolution for numerical modeling.

The governing equations including the mass, momentum and energy conservation equations are given as:

$$\nabla \cdot (\rho \mathbf{u}) = 0$$

$$\rho C \left( \frac{\partial T}{\partial t} + \mathbf{u} \cdot \nabla T \right) = \nabla \cdot (k \nabla T)$$

$$\frac{\partial \rho \mathbf{u}}{\partial t} + \nabla \cdot (\rho \mathbf{u} \otimes \mathbf{u}) = -\nabla P + \mu \nabla^2 \mathbf{u} + \rho \mathbf{g},$$

where  $\rho$ ,  $C$ ,  $k$ , and  $\mu$  are the mass density, specific heat, thermal conductivity, and dynamic viscosity of the molten polymer,  $t$  is time, and  $\mathbf{u}$ ,  $T$ ,  $P$ , and  $\mathbf{g}$  are the flow velocity vector, temperature, pressure, and gravitational acceleration vector, respectively. Particularly the dynamic viscosity is dependent on the local strain rate and temperature, which is measured in experiments. The simulations are conducted using the commercial software Flow3D.

### Single eco-voxel mechanical characterization

Compression tests of individual eco-voxels were performed on a model 3400 universal mechanical testing machine (Instron), using a 5-kN load cell, equipped with an AVE 2 video extensometer (Instron) at an extension rate of 10 mm/min. Bluehill software was used for data acquisition (Figure S2).

### Structural performance simulation, analysis, and optimization

To assess the structural performance of eco-voxel lattices with side lengths of up to three voxels (Figure 2) finite element analysis (FEA) simulations were conducted using full 3D models. The considered eco-voxel dimensions are listed in Table 4. SolidWorks 3D computer-aided design application software (Dassault Systemes, Waltham, MA, USA) was used for the eco-voxel design. To create the 2 × 2 × 2, 3 × 3 × 3 eco-voxel lattices and the eco-voxel lattice wall, we used mirroring as eco-voxels are symmetric. Following the 3D model design, a high-fidelity discretization in Hypermesh finite element modeling and analysis software (Altair, Troy, MI, USA) was performed. Stress quadratic tetrahedral elements (element type C3D10) were employed, resulting in approximately 80,000 elements per eco-voxel. The discretized model was then imported into Abaqus software (Dassault Systemes, Johnston, RI, USA). The boundary conditions for the simulations were (1) the bottom surface of the first layer of the eco-voxel structure was fixed, and (2) the top surface was free to rotate and displace in any direction. To prevent non-convergencies, a displacement control approach was used, and a pre-defined displacement was applied at the top surface to achieve compression.<sup>51</sup> The ROM simulations of the 2 × 2 × 2 and 3 × 3 × 3 eco-voxel lattices (Figure 2), as well as the eco-voxel wall (Figure 3), were implemented on Abaqus using Timoshenko beam elements (3-node quadratic Timoshenko beam, B32). Each strut was discretized into 10 shear-deformable beam elements with a uniform cross-section. A mesh sensitivity analysis ensured that the number of elements achieved convergence, and the results were validated against

the more accurate full 3D model (Note S5 and Figure S7). All simulations used the Abaqus explicit solver with geometric nonlinearity enabled. For computational simplicity, the PTT + rCF material's slight stress-strain (Figure S6I) nonlinearity was neglected, and the pre-yield behavior was approximated as linear elastic.

To evaluate the structural performance of the eco-voxel wall, we considered load requirements for a load-bearing wall in a single-story residential light-frame construction in the United States, following ASCE7 standards.<sup>26</sup> The wall was designed to support vertical compressive forces ( $V$ ), which include one-half the roof load, one-half the snow load, and a safety factor of 2, as well as lateral forces due to wind pressure ( $W$ ). The roof is assumed to be designed as a sandwich composite, consisting of an eco-voxel inner layer and two 65-mm-thick CLT layers. Each voxel features a conservative mass of 31.5 g including the metallic fasteners and there are 169 voxels in an area of 1 m<sup>2</sup> leading to a voxel load of 52.16 N/m<sup>2</sup>. Each CLT layer, with a density of 485 kg/m<sup>3</sup>, contributes 309.26 N/m<sup>2</sup>, resulting in a total CLT load of 618.52 N/m<sup>2</sup>. Summing up both contributions, the total estimated dead-load is approximately  $D = 670$  N/m<sup>2</sup>. A snow load of 2,400 N/m<sup>2</sup> was used, reflecting conditions typical of northern U.S. regions. Wind load calculations were based on a design wind speed of 32 m/s for Massachusetts, with a lateral wall pressure coefficient of 1.1 leading to a value of  $W = 680$  N/m<sup>2</sup> (worst-case scenario). The distributed vertical ( $V$ ) and lateral ( $W$ ) design loads are summarized in Table 4.

### Sustainability assessment

The GHG emissions and the mass of the eco-voxel wall were compared with those of a concrete masonry wall, a 3D-printed concrete wall, and a CLT wall of similar load-bearing capacities. To calculate the GHG emissions associated with each wall system, a life cycle analysis approach was followed in accordance with the International Organization for Standardization standards 14040<sup>86</sup> and 14044,<sup>87</sup> utilizing a cradle-to-gate system boundary. This boundary considers the environmental impacts from raw material extraction, processing, and manufacturing, but excludes the transportation, construction, use, and end-of-life phases of the different walls. The functional unit used is 1 m<sup>2</sup> of external load-bearing wall in a single-story residential building, designed to meet the equivalent load-bearing capacities of each wall type, based on the ASCE 7 standard.<sup>26</sup> This ensures that the structural capacities of the walls are comparable while assessing their environmental impact.

Data from literature sources and the ecoinvent 3.9.1 database<sup>88</sup> were used, applying the cutoff system model for global geographies. Greenhouse gas emissions, expressed in kilograms of CO<sub>2</sub>-eq, were assessed based on global warming potentials over a 100-year time horizon, following the IPCC 2021 methodology.<sup>89</sup> More specifically, the GHG emissions of PTT were calculated based on information provided by Dupont<sup>35</sup> and Kurian,<sup>30</sup> while the GHG emissions of rCF reclaimed through pyrolysis recycling, as reported by Meng et al.<sup>43</sup> were considered. Injection molding and PU emissions were sourced from ecoinvent.

The concrete wall is constructed from hollow concrete masonry blocks, reinforced by two concrete columns and one

beam with steel rebar, with a thickness of 30 cm. The dimensions of the columns, beam, and the quantities of mortar, concrete, and reinforcing steel per square meter of wall were based on Mohammad et al.<sup>91</sup> and adjusted for the 30-cm wall thickness. Plywood for formwork was excluded from the analysis, as it can be reused multiple times and its contribution to total GHG emissions was expected to be minimal. The wall utilizes 4 MPa hollow concrete blocks (dimensions: 140 mm width, 390 mm length, and 190 mm height) with an average mass of 12.4 kg. The concrete used is 40 MPa ready-mix concrete, with a density of 2,453 kg/m<sup>3</sup> and a water-to-cement ratio of 0.55. The concrete's composition per m<sup>3</sup> includes 380 kg of type ICo cement, 195 kg of water, 1,116 kg of gravel, 744 kg of sand, and 3.8 kg of admixtures (0.3% retarder and 0.7% superplasticizers by cement weight). These quantities were adjusted based on the wall's dimensions.

For the 3D-printed concrete wall, with a thickness of 0.30 m (including voids), is made from a high-performance concrete consisting of ordinary Portland cement, fly ash, river sand, polypropylene microfibers, alkali-free accelerators, and superplasticizers. Material quantities were based on those reported by Mohammad et al.<sup>91</sup> Data for Portland cement, concrete plasticizer (sulfonated melamine formaldehyde), deionized water, and polypropylene production were sourced from the ecoinvent database, while the remaining data were taken from Mohammad et al.<sup>91</sup>

Ecoinvent data were also used for the CLT wall of 0.50 m width.

### RESOURCE AVAILABILITY

#### Lead contact

Requests for further information and resources should be directed to and will be fulfilled by the lead contact, Christos E. Athanasiou ([athanasiou@gatech.edu](mailto:athanasiou@gatech.edu)).

#### Materials availability

The materials generated in this study are available from the corresponding author upon request.

#### Data and code availability

- The data that support the findings of this study are available within the article and its supplemental material.
- Any additional information required to reanalyze the data reported in this paper is available from the [lead contact](#) upon reasonable request.

### ACKNOWLEDGMENTS

D.G. and C.E.A. acknowledge support from the National Science Foundation (NSF) CAREER Award [CMMI-2338508]. C.E.A. acknowledges useful discussions on sustainability assessment with Patricia Stathatou (Georgia Tech, School of Chemical and Biomolecular Engineering). The simulations were conducted using the Advanced Computing Environment (PACE) at the Georgia Institute of Technology, Atlanta, Georgia, USA.

### AUTHOR CONTRIBUTIONS

Conceptualization and supervision, C.E.A.; mechanical testing, injection molding experiments, structural simulations, and sustainability assessment, D.G., and D.O.; thermomechanical simulations, Z.Y. and W.Y.; material development, T.W., M.R.S., and A.M.; writing, all authors.

## DECLARATION OF INTERESTS

The authors declare no competing interests.

## SUPPLEMENTAL INFORMATION

Supplemental information can be found online at <https://doi.org/10.1016/j.matt.2025.102106>.

Received: December 17, 2024

Revised: March 4, 2025

Accepted: March 20, 2025

Published: April 11, 2025

## REFERENCES

1. Congressional Budget Office (2024). Climate Change, Disaster Risk, and Homeowner's Insurance
2. World Bank Open Data (2018). Population living in slums: Retrieved from <https://data.worldbank.org/indicator/EN.POP.SLUM.UR.ZS>.
3. McKinsey Global Institute (2014). A blueprint for addressing the global affordable housing challenge Executive summary.
4. Harvard Joint Center for Housing Studies (2019). The State of the Nation's Housing 2019.
5. United Nations Environment Programme (UNEP) (2022). 2022 Global Status Report for Buildings and Construction: Towards a zero-emissions, efficient and resilient buildings and construction sector.
6. Gregory, J., AzariJafari, H., Vahidi, E., Guo, F., Ulm, F.-J., and Kirchain, R. (2021). The role of concrete in life cycle greenhouse gas emissions of US buildings and pavements. *Proc. Natl. Acad. Sci. USA*, 118. e2021936118, <https://doi.org/10.1073/pnas.2021936118>.
7. Editorial (2021). Concrete needs to lose its colossal carbon footprint. *Nature* 597, 593–594. <https://doi.org/10.1038/d41586-021-02612-5>.
8. Andrew, R.M. (2018). Global CO2 emissions from cement production. *Earth Syst. Sci. Data* 10, 195–217. <https://doi.org/10.5194/essd-10-195-2018>.
9. US EPA Website (2021). Sustainable Management of Construction and Demolition Materials. Retrieved from: <https://www.epa.gov/smm/sustainable-management-construction-and-demolition-materials>.
10. Loizou, L., Barati, K., Shen, X., and Li, B. (2021). Quantifying Advantages of Modular Construction: Waste Generation. *Buildings* 11, 622. <https://doi.org/10.3390/buildings11120622>.
11. The Modular Buildings Institute (2024). 2024 Annual Report: Key Financial Data and Metrics for the Relocatable buildings industry, Retrieved from: <https://www.modular.org/industry-analysis/>.
12. Hiller, J., and Lipson, H. (2009). Design and analysis of digital materials for physical 3D voxel printing. *Rapid Prototyp. J.* 15, 137–149. <https://doi.org/10.1108/13552540910943441>.
13. Cheung, K.C., and Gershenfeld, N. (2013). Reversibly Assembled Cellular Composite Materials. *Science* 341, 1219–1221. <https://doi.org/10.1126/science.1240889>.
14. Jenett, B., Cameron, C., Tourlomousis, F., Rubio, A.P., Ochalek, M., and Gershenfeld, N. (2020). Discretely assembled mechanical metamaterials. *Sci. Adv.* 6, 9943–9961. <https://doi.org/10.1126/sciadv.abc9943>.
15. Jenett, B., Cellucci, D., Gregg, C., and Cheung, K. (2016). Meso-Scale Digital Materials: Modular, Reconfigurable, Lattice-Based Structures. In Volume 2: Materials; Biomanufacturing; Properties, Applications and Systems; Sustainable Manufacturing (American Society of Mechanical Engineers). <https://doi.org/10.1115/MSEC2016-8767>.
16. Jenett, B.E. (2020). *Discrete Mechanical Metamaterials* (Massachusetts Institute of Technology).
17. Gregg, C.E., Catanoso, D., Formoso, O.I.B., Kostitsyna, I., Ochalek, M.E., Olatunde, T.J., Park, I.W., Sebastianelli, F.M., Taylor, E.M., Trinh, G.T., and Cheung, K.C. (2024). Ultralight, strong, and self-reprogrammable mechanical metamaterials. *Sci. Robot.* 9, eadi2746. <https://doi.org/10.1126/scirobotics.adi2746>.
18. Alhumayani, H., Gomaa, M., Soebarto, V., and Jabi, W. (2020). Environmental assessment of large-scale 3D printing in construction: A comparative study between cob and concrete. *J. Clean. Prod.* 270, 122463. <https://doi.org/10.1016/j.jclepro.2020.122463>.
19. Robbins, J. (2019). As Mass Timber Takes off, How Green Is This New Building Material? (Yale School of the Environment). Retrieved from <https://e360.yale.edu/features/as-mass-timber-takes-off-how-green-is-this-new-building-material>.
20. Georgiou, D., Sun, D., Liu, X., and Athanasiou, C.E. (2025). Suppressing Mechanical Property Variability in Recycled Plastics via Bio-inspired Design. Preprint at arXiv. <https://doi.org/10.48550/arXiv.2502.02359>.
21. Athanasiou, C.E., Liu, X., and Gao, H. (2024). A Perspective on Democratizing Mechanical Testing: Harnessing Artificial Intelligence to Advance Sustainable Material Adoption and Decentralized Manufacturing. *J. Appl. Mech.* 91, 110801. <https://doi.org/10.1115/1.4066085>.
22. Athanasiou, C.E., Deng, B., and Hassen, A.A. (2024). Integrating Experiments, Simulations, and Artificial Intelligence to Accelerate the Discovery of High-Performance Green Composites. In AIAA SCITECH 2024 Forum (American Institute of Aeronautics and Astronautics). <https://doi.org/10.2514/6.2024-0041>.
23. Stathatou, P.M., Corbin, L., Meredith, J.C., and Garmulewicz, A. (2023). Biomaterials and Regenerative Agriculture: A Methodological Framework to Enable Circular Transitions. *Sustainability* 15, 14306. <https://doi.org/10.3390/su151914306>.
24. Andrew, J.J., and Dhakal, H.N. (2022). Sustainable biobased composites for advanced applications: recent trends and future opportunities – A critical review. *Composites Part C: Open Access* 7, 100220. <https://doi.org/10.1016/j.jcocom.2021.100220>.
25. Li, M., Pu, Y., Thomas, V.M., Yoo, C.G., Ozcan, S., Deng, Y., Nelson, K., and Ragauskas, A.J. (2020). Recent advancements of plant-based natural fiber-reinforced composites and their applications. *Compos. B Eng.* 200, 108254. <https://doi.org/10.1016/j.compositesb.2020.108254>.
26. American Society of Civil Engineers (2022). Minimum design loads and associated criteria for buildings and other structures : provisions.
27. Ashby, M.F. (2013). *Materials and the Environment* (Elsevier). <https://doi.org/10.1016/C2010-0-66554-0>.
28. Greendot Bioplastics Terratek® WC/SC/HC/CC - Technical Data Sheet.
29. Mitsubishi Chemical Group Ketron® Sterra™ 1000 PEEK - Technical Data Sheet.
30. The Resin Enterprise Inc. Recycled PEEK® - Report.
31. NatureWorks Ingeo™ Biopolymer 3052D - Technical Data Sheet.
32. Mango Materials Retrieved From: <https://www.mangomaterials.com>.
33. Dalton, B., Bhagabati, P., De Micco, J., Padamati, R.B., and O'Connor, K. (2022). A Review on Biological Synthesis of the Biodegradable Polymers Polyhydroxyalkanoates and the Development of Multiple Applications. *Catalysts* 12, 319. <https://doi.org/10.3390/catal12030319>.
34. DuPont DuPont™ Zytel® 70G33L BK031 Nylon 66 - Technical Data Sheet, Retrieved from: [https://www.matweb.com/search/datasheet\\_print.aspx?matguid=2448fb82feb544f6a2677def4e0fbd31](https://www.matweb.com/search/datasheet_print.aspx?matguid=2448fb82feb544f6a2677def4e0fbd31).
35. DuPont DuPont™ Sorona® FG3301 NC010 - Technical Data Sheet.
36. Barmet Barmet-carbon™ CF82PU® - Technical Data Sheet.
37. Zhang, Z.-Z., Song, H.-J., Men, X.-H., and Luo, Z.-Z. (2008). Effect of carbon fibers surface treatment on tribological performance of polyurethane (PU) composite coating. *Wear* 264, 599–605. <https://doi.org/10.1016/j.wear.2007.05.003>.
38. Zhang, T., Zhao, Y., Li, H., and Zhang, B. (2018). Effect of polyurethane sizing on carbon fibers surface and interfacial adhesion of fiber/polyamide 6 composites. *J. Appl. Polym. Sci.* 135. <https://doi.org/10.1002/app.46111>.
39. Kobayashi, T., Wood, B.A., Blackman, G.S., and Takemura, A. (2011). Morphology, dynamic mechanical, and electrical properties of bio-based

- poly(trimethylene terephthalate) blends, part 1: Poly(trimethylene terephthalate)/poly(ether esteramide)/polyethylene glycol 400 bis(2-ethylhexanoate) blends. *J. Appl. Polym. Sci.* *120*, 3519–3529. <https://doi.org/10.1002/app.33498>.
40. Enriquez, E., Mohanty, A.K., and Misra, M. (2016). Biobased polymer blends of poly(trimethylene terephthalate) and high density polyethylene. *Mater. Des.* *90*, 984–990. <https://doi.org/10.1016/j.matdes.2015.10.066>.
41. Kobayashi, T., Wood, B.A., and Takemura, A. (2011). Crystallization, morphology, and electrical properties of bio-based poly(trimethylene terephthalate)/poly(ether esteramide)/ionomer blends. *J. Appl. Polym. Sci.* *119*, 2714–2724. <https://doi.org/10.1002/app.32945>.
42. Kobayashi, T., Wood, B.A., and Takemura, A. (2012). Morphology, dynamic mechanical, and electrical properties of bio-based poly(trimethylene terephthalate) blends, part 2: Poly(trimethylene terephthalate)/poly(ether esteramide)/polycarbonate blends. *J. Appl. Polym. Sci.* *123*, 1056–1067. <https://doi.org/10.1002/app.34571>.
43. Meng, F., Olivetti, E.A., Zhao, Y., Chang, J.C., Pickering, S.J., and McKechnie, J. (2018). Comparing Life Cycle Energy and Global Warming Potential of Carbon Fiber Composite Recycling Technologies and Waste Management Options. *ACS Sustain. Chem. Eng.* *6*, 9854–9865. <https://doi.org/10.1021/acssuschemeng.8b01026>.
44. Gregg, C.E., Kim, J.H., and Cheung, K.C. (2018). Ultra-Light and Scalable Composite Lattice Materials. *Adv. Eng. Mater.* *20*. <https://doi.org/10.1002/adem.201800213>.
45. Liu, W., Mohanty, A.K., Drzal, L.T., Misra, M., Kurian, J.V., Miller, R.W., and Strickland, N. (2005). Injection molded glass fiber reinforced poly(trimethylene terephthalate) composites: Fabrication and properties evaluation. *Ind. Eng. Chem. Res.* *44*, 857–862. <https://doi.org/10.1021/ie049112f>.
46. Vivekanandhan, S., Misra, M., and Mohanty, A.K. (2012). Thermal, mechanical, and morphological investigation of injection molded poly(trimethylene terephthalate)/carbon fiber composites. *Polym. Compos.* *33*, 1933–1940. <https://doi.org/10.1002/pc.22333>.
47. Page, I.B. (2000). *Polyamides as Engineering Thermoplastic Materials, 1st ed.* (Rapra Technology LTD).
48. Rimoli, J.J. (2018). A reduced-order model for the dynamic and post-buckling behavior of tensegrity structures. *Mech. Mater.* *116*, 146–157. <https://doi.org/10.1016/j.mechmat.2017.01.009>.
49. Pajunen, K., Johanns, P., Pal, R.K., Rimoli, J.J., and Daraio, C. (2019). Design and impact response of 3D-printable tensegrity-inspired structures. *Mater. Des.* *182*, 107966. <https://doi.org/10.1016/j.matdes.2019.107966>.
50. Lee, S., Zhang, Z., and Gu, G.X. (2022). Generative machine learning algorithm for lattice structures with superior mechanical properties. *Mater. Horiz.* *9*, 952–960. <https://doi.org/10.1039/d1mh01792f>.
51. Chen, E., Luan, S., and Gaitanaros, S. (2022). On the compressive strength of brittle lattice metamaterials. *Int. J. Solids Struct.* *257*, 111871. <https://doi.org/10.1016/j.ijsolstr.2022.111871>.
52. Portela, C.M., Greer, J.R., and Kochmann, D.M. (2018). Impact of node geometry on the effective stiffness of non-slender three-dimensional truss lattice architectures. *Extreme Mech. Lett.* *22*, 138–148. <https://doi.org/10.1016/j.eml.2018.06.004>.
53. Mueller, J., Matlack, K.H., Shea, K., and Daraio, C. (2019). Energy Absorption Properties of Periodic and Stochastic 3D Lattice Materials. *Adv. Theory Simul.* *2*. <https://doi.org/10.1002/adts.201900081>.
54. Zhang, X., Vyatskikh, A., Gao, H., Greer, J.R., and Li, X. (2019). Lightweight, flaw-tolerant, and ultrastrong nanoarchitected carbon. *Proc. Natl. Acad. Sci. USA* *116*, 6665–6672. <https://doi.org/10.1073/pnas.1817309116>.
55. Tancogne-Dejean, T., and Mohr, D. (2018). Elastically-isotropic truss lattice materials of reduced plastic anisotropy. *Int. J. Solids Struct.* *138*, 24–39. <https://doi.org/10.1016/j.ijsolstr.2017.12.025>.
56. Deshpande, V.S., Ashby, M.F., and Fleck, N.A. (2001). Foam topology: bending versus stretching dominated architectures. *Acta Mater.* *49*, 1035–1040. [https://doi.org/10.1016/S1359-6454\(00\)00379-7](https://doi.org/10.1016/S1359-6454(00)00379-7).
57. Gong, C., Ritchie, R.O., Wei, X., Liu, Q., and Xiong, J. (2025). Mechanical properties of modular assembled composite lattice architecture. *J. Mech. Phys. Solids* *195*, 105967. <https://doi.org/10.1016/j.jmps.2024.105967>.
58. Ashby, M.F. (2006). The properties of foams and lattices. *Philos. Trans. A Math. Phys. Eng. Sci.* *364*, 15–30. <https://doi.org/10.1098/rsta.2005.1678>.
59. Jenett, B., G. Neil, C. Kenneth, and G. Christine (2024). Cuboctahedron lattice materials.
60. Ryvkin, M., Slesarenko, V., Cherkaev, A., and Rudykh, S. (2020). Fault-tolerant elastic-plastic lattice material. *Philos. Trans. A Math. Phys. Eng. Sci.* *378*, 20190107. <https://doi.org/10.1098/rsta.2019.0107>.
61. Tankasala, H.C., Deshpande, V.S., and Fleck, N.A. (2017). Tensile response of elastoplastic lattices at finite strain. *J. Mech. Phys. Solids* *109*, 307–330. <https://doi.org/10.1016/j.jmps.2017.02.002>.
62. Kundu, R.D., and Zhang, X.S. (2025). Sustainability-oriented multimaterial topology optimization: designing efficient structures incorporating environmental effects. *Struct. Multidiscipl. Optim.* *68*, 17. <https://doi.org/10.1007/s00158-024-03930-8>.
63. Mohanty, A.K., Vivekanandhan, S., Pin, J.-M., and Misra, M. (2018). Composites from renewable and sustainable resources: Challenges and innovations. *Science* *362*, 536–542. <https://doi.org/10.1126/science.aat9072>.
64. Silverman, E.M. (1987). Effect of glass fiber length on the creep and impact resistance of reinforced thermoplastics. *Polym. Compos.* *8*, 8–15. <https://doi.org/10.1002/pc.750080103>.
65. Liu, H., Yin, L., Wu, D., Yao, Z., Zhang, M., Chen, C., Fu, P., and Qin, J. (2015). Mechanical properties and creep behavior of poly(trimethylene terephthalate)/mesoporous silica composites. *Polym. Compos.* *36*, 1386–1393. <https://doi.org/10.1002/pc.23043>.
66. Liu, X., Athanasiou, C.E., Pature, N.P., Sheldon, B.W., and Gao, H. (2021). Knowledge extraction and transfer in data-driven fracture mechanics. *Proc. Natl. Acad. Sci. USA* *118*, e2104765118. <https://doi.org/10.1073/pnas.2104765118>.
67. Nazir, S.I., Athanasiou, C.E., and Bellouard, Y. (2022). On the behavior of uniaxial static stress loaded micro-scale fused silica beams at room temperature. *J. Non-Cryst. Solids X* *14*, 100083. <https://doi.org/10.1016/j.nocx.2022.100083>.
68. Athanasiou, C.E., Fincher, C.D., Gilgenbach, C., Gao, H., Carter, W.C., Chiang, Y.-M., and Sheldon, B.W. (2024). Operando measurements of dendrite-induced stresses in ceramic electrolytes using photoelasticity. *Matter* *7*, 95–106. <https://doi.org/10.1016/j.matt.2023.10.014>.
69. Athanasiou, C.E., Liu, X., Zhang, B., Cai, T., Ramirez, C., Pature, N.P., Lou, J., Sheldon, B.W., and Gao, H. (2023). Integrated simulation, machine learning, and experimental approach to characterizing fracture instability in indentation pillar-splitting of materials. *J. Mech. Phys. Solids* *170*, 105092. <https://doi.org/10.1016/j.jmps.2022.105092>.
70. Athanasiou, C.E., and Bellouard, Y. (2015). A Monolithic Micro-Tensile Tester for Investigating Silicon Dioxide Polymorph Micromechanics, Fabricated and Operated Using a Femtosecond Laser. *Micromachines* *6*, 1365–1386. <https://doi.org/10.3390/mi6091365>.
71. Yi, R., Georgiou, D., Liu, X., and Athanasiou, C.E. (2025). Mechanics-informed, model-free symbolic regression framework for solving fracture problems. *J. Mech. Phys. Solids* *194*, 105916. <https://doi.org/10.1016/j.jmps.2024.105916>.
72. Astute Analytical (2024). Global Recycled Carbon Fiber Market: By Type (Chopped Recycled Carbon Fiber and Milled Recycled Carbon Fiber); Source (Automotive, Aerospace, and Others); Process (Pyrolysis and Solvolysis); Application (Automotive, Wind Energy, Civil Engineering, 3D Printing, Energy Storage, Sporting Goods, Marine, Thermoplastic Compounding, Oil & Gas, Pressure Vessels, Aerospace and Defense, and Others); Region—Market Size, Industry Dynamics, Opportunity Analysis and Forecast for 2024–2032. .
73. Globe Newswire (2024). Global Carbon Fiber Market to Hit Market Size of USD 52.16 Billion by 2050 (Astute Analytica). Retrieved from: <https://www>.

- [globenewswire.com/news-release/2024/04/03/2857049/0/en/Global-Carbon-Fiber-Market-to-Hit-Market-Size-of-USD-52-16-Billion-By-2050-Astute-Analytica.html](https://globenewswire.com/news-release/2024/04/03/2857049/0/en/Global-Carbon-Fiber-Market-to-Hit-Market-Size-of-USD-52-16-Billion-By-2050-Astute-Analytica.html).
74. Grand View Research Inc (2020). Polytrimethylene Terephthalate Market Size, Share & Trends Analysis Report By End-use (Automotive, Textiles), By Type (Petroleum, Bio-based), By Application (Film Materials, Fiber), By Region, And Segment Forecasts, 2022 - 2030. Retrieved from: <https://www.grandviewresearch.com/industry-analysis/polytrimethylene-terephthalate-market>.
  75. Fact.MR (2024). Polytrimethylene Terephthalate Market. Retrieved from: <https://www.factmr.com/report/polytrimethylene-terephthalate-market>.
  76. Al-Homoud, M.S. (2005). Performance characteristics and practical applications of common building thermal insulation materials. *Build. Environ.* *40*, 353–366. <https://doi.org/10.1016/j.buildenv.2004.05.013>.
  77. Hung Anh, L.D., and Pásztor, Z. (2021). An overview of factors influencing thermal conductivity of building insulation materials. *J. Build. Eng.* *44*, 102604. <https://doi.org/10.1016/j.jobbe.2021.102604>.
  78. Dickson, T., and Pavia, S. (2021). Energy performance, environmental impact and cost of a range of insulation materials. *Renew. Sustain. Energy Rev.* *140*, 110752. <https://doi.org/10.1016/j.rser.2021.110752>.
  79. ASTM Standard D618 (2021). Standard Practice for Conditioning Plastics for Testing (ASTM International). <https://doi.org/10.1520/D0618-21>. [www.astm.org](http://www.astm.org).
  80. ASTM Standard D638 (2014). Standard Test Method for Tensile Properties of Plastics (ASTM International). <https://doi.org/10.1520/D0638-14>. [www.astm.org](http://www.astm.org).
  81. ASTM Standard D790 (2017). Standard Test Methods for Flexural Properties of Unreinforced and Reinforced Plastics and Electrical Insulating Materials (ASTM International). <https://doi.org/10.1520/D0790-17>. [www.astm.org](http://www.astm.org).
  82. ASTM Standard D256, 2023e1 (2023). Standard Test Methods for Determining the Izod Pendulum Impact Resistance of Plastics (ASTM International). <https://doi.org/10.1520/D0256-23E01>. [www.astm.org](http://www.astm.org).
  83. ASTM Standard D648 (2018). Standard Test Method for Deflection Temperature of Plastics under Flexural Load in the Edgewise Position (ASTM International). <https://doi.org/10.1520/D0648-18>. [www.astm.org](http://www.astm.org).
  84. Bid Wadud, S.E., and Ullbrich, R.R. Using the DMA Q800 for ASTM International D 648 Deflection Temperature Under Load.
  85. ASTM Standard D1238 (2023). Standard Test Method for Melt Flow Rates of Thermoplastics by Extrusion Plastometer (ASTM International). <https://doi.org/10.1520/D1238-23A>. [www.astm.org](http://www.astm.org).
  86. International Organization for Standardization (ISO). INTERNATIONAL STANDARD ISO 14040: Environmental Management — Life Cycle Assessment — Principles and Framework, 2006.
  87. International Organization for Standardization (ISO). INTERNATIONAL STANDARD ISO 14044: Environmental Management — Life Cycle Assessment — Requirements and Guidelines, 2006.
  88. Wernet, G., Bauer, C., Steubing, B., Reinhard, J., Moreno-Ruiz, E., and Weidema, B. (2016). The ecoinvent database version 3 (part I): overview and methodology. *Int. J. Life Cycle Assess.* *21*, 1218–1230. <https://doi.org/10.1007/s11367-016-1087-8>.
  89. IPCC (2021). Sixth Assessment Report (AR6), Retrieved from. <https://www.ipcc.ch/assessment-report/ar6/>.
  90. Kurian, J.V. (2005). A New Polymer Platform for the Future — Sorona® from Corn Derived 1,3-Propanediol. *J. Polym. Environ.* *13*, 159–167. <https://doi.org/10.1007/s10924-005-2947-7>.
  91. Mohammad, M., Masad, E., and Al-Ghamdi, S.G. (2020). 3d concrete printing sustainability: A comparative life cycle assessment of four construction method scenarios. *Buildings* *10*, 245–320. <https://doi.org/10.3390/buildings10120245>.